

# Dispatch-Aware Deep Neural Network for Optimal Transmission Switching

Minsoo Kim, *Member, IEEE*, Andy Sun, *Senior Member, IEEE*, and Jip Kim, *Member, IEEE*

**Abstract**—Optimal transmission switching (OTS) improves optimal power flow (OPF) by selectively opening transmission lines, but its mixed-integer formulation increases computational complexity, especially on large grids. To deal with this, we propose a dispatch-aware deep neural network (DA-DNN) that accelerates DC-OTS without relying on pre-solved labels. DA-DNN predicts line states and passes them through an embedded differentiable DC-OPF layer, using the resulting generation cost as the loss function so that all physical network constraints are enforced throughout training and inference. In addition, we adopt a customized weight-bias initialization that keeps every forward pass feasible from the first iteration, which allows stable learning. Once trained, the proposed DA-DNN successfully produces a feasible topology and dispatch pair in the same time as solving the DCOPF, whereas conventional mixed-integer solvers become intractable. Moreover, the embedded OPF layer enables DA-DNN to generalize to untrained system configurations, such as changes in line flow limits. As a result, the proposed method successfully captures the economic advantages of OTS while maintaining scalability and generalization ability.

## SELECTED NOMENCLATURE

### A. Variables

$\mathbf{p}_g, \mathbf{z}, \boldsymbol{\theta}$	Optimization variables
$\hat{\mathbf{p}}_g, \hat{\mathbf{z}}, \hat{\boldsymbol{\theta}}$	Predicted variables (from neural network)
$\mathbf{p}_g^*, \mathbf{z}^*, \boldsymbol{\theta}^*$	Optimized variables
$\bar{\mathbf{z}}$	Input of last layer of neural network
$\bar{\mathbf{z}}$	Binarized line status
$\phi$	Learnable parameters of neural network
$\mathbf{W}, \mathbf{b}$	Weight and bias of neural network
$\mathbf{W}^{\text{last}}, \mathbf{b}^{\text{last}}$	Weight and bias of last layer of neural network
$\mathbf{W}_{\text{init}}^{\text{last}}, \mathbf{b}_{\text{init}}^{\text{last}}$	Initial value of $\mathbf{W}^{\text{last}}, \mathbf{b}^{\text{last}}$

### B. Functions

$\mathcal{L}$	Loss function
$C$	Generation cost function
$\text{diag}$	Diagonalization function
$L$	Lagrange function
$f, g, h$	Objective/inequality/equality function of $L$
$\Phi$	Neural network model
$B$	Binarization function

### C. Parameters

$N_b, N_g, N_l$	The number of buses, generators, and lines
$T$	Maximum training epochs
$\mathbf{M}$	Generator-bus incidence matrix
$\mathbf{C}$	Branch-bus incidence matrix

$\bar{\mathbf{p}}_g, \underline{\mathbf{p}}_g$	Generation limits
$\bar{\boldsymbol{\theta}}, \underline{\boldsymbol{\theta}}$	Voltage angle limits
$\bar{\mathbf{p}}_l, \underline{\mathbf{p}}_l$	line flow limits
$\bar{\mathbf{p}}_{l,z}, \underline{\mathbf{p}}_{l,z}$	line flow limits with switching
$\mathbf{b}_l, \underline{\mathbf{b}}_{l,z}$	Line susceptance with/without switching
$\mathbf{p}_d$	Bus demand
$\lambda$	Lagrange multiplier of equality constraints
$\mu$	Lagrange multiplier of inequality constraints
$\Phi$	Neural network model
$\eta_{\text{lr}}$	Learning rate

## I. INTRODUCTION

Optimal transmission switching (OTS) strategically opens or closes transmission lines so that the network topology becomes an active control variable [1]. By doing so, system operators can reroute power flows and reduce generation costs. This effect is known as Braess's paradox in power systems, where removing a line can redirect flows and reduce the total operational cost [2]. Beyond this counterintuitive phenomenon, OTS provides a practical mechanism for alleviating congestion, accessing cheaper generation, and improving system flexibility without building new infrastructure. This is because treating the line status as a decision variable enlarges the feasible set and enables more cost-effective dispatch solutions from an optimization perspective.

Pilot studies show that transmission switching can deliver significant economic and reliability improvements in real power grids. For example, simulations from the ARPA-E Topology Control Algorithm project indicate that transmission switching in the PJM system can reduce congestion costs by more than 50% and save over 100 million USD annually in the real-time market [3]. In addition, ERCOT has used transmission switching to replace post-contingency load shedding and to support more effective corrective and preventive operating plans [4]. Beyond PJM, several system operators have reported that even a single transmission switching action can yield significant operational benefits. For example, in MISO, a single switching action applied during a 345-kV outage reduced regional wind curtailments by 86% and reduced congestion costs by 3.5 million USD [5]. In SPP, a real-time operational pilot study found that single switching actions could provide more than 25% flow reduction [4]. These results demonstrate that even minimal transmission switching adjustments can provide substantial operational value in real-world systems.

Recognizing the operational benefits of topology switching, regulatory and policy have begun to encourage its evaluation

TABLE I. COMPARISON OF OTS METHODOLOGIES.

Work	Methodology	Unsupervised learning	Feasibility of dispatch	Evaluation under untrained constraints
Ruiz <i>et al.</i> [6]	Heuristic	✗	✓	✗
Fuller <i>et al.</i> [7]	Heuristic	✗	✓	✗
Hedman <i>et al.</i> [8]	Heuristic	✗	✓	✗
Barrows <i>et al.</i> [9]	Heuristic	✗	✓	✗
Jabarnejad <i>et al.</i> [10]	Heuristic	✗	✓	✗
Han <i>et al.</i> [11]	Learning-based	✗	✗	✗
Lehna <i>et al.</i> [12]	Learning-based	✗	✗	✗
Tang <i>et al.</i> [13]	Learning-based	✗	✗	✗
Pineda <i>et al.</i> [14]	Learning-based	✓	✗	✗
Bugaje <i>et al.</i> [15]	Learning-based	✓	✓	✗
Yang <i>et al.</i> [16]	Learning-based	✓	✗	✗
<b>DA-DNN (proposed)</b>	Learning-based	✓	✓	✓

alongside other grid-enhancing technologies. For example, FERC Order No. 1920 in the United States and ENTSO-E's Research and Innovation Roadmap 2017–2026 in Europe explicitly identify transmission switching as an option to improve grid flexibility and operational efficiency [17], [18]. In parallel with this regulatory momentum, system operators such as PJM and ISO-NE already employ limited corrective switching during contingencies to alleviate overloads and maintain reliability [19], [20].

Although there is a huge potential in OTS, its adoption in practice has been hindered by high computational complexity [21]. Specifically, transmission switchings examined in these studies [3]–[5] are not obtained by solving full OTS and therefore capture only a small portion of the possible benefits. Fully exploiting the value of transmission switching requires obtaining globally optimal transmission switching decisions by introducing binary line status of optimization variables. By doing so, OPF problem is transformed into a mixed integer program that is NP hard and often intractable for large networks [22]. Commercial solvers may take minutes to days or fail to converge entirely, which prevents OTS from being used in both day-ahead and real-time operations. Thus, faster OTS solution methods are essential, and a variety of approaches have been explored to accelerate computation, as summarized in Table I.

One major direction is the use of heuristic algorithms that construct high quality switching decisions without exhaustively solving the full MIP. Early works on OTS focused on heuristic approaches that reduce computation by narrowing the search over switching actions. These methods typically rely on the structural features of the power system or simplified representations of problems. Sensitivity-based methods rank candidate lines using power transfer distribution factors or shadow prices [6], while other studies rely on OPF-derived congestion indicators [7]. Greedy heuristic algorithm iteratively open lines to reduce cost, as in [8]. Topological metrics have been tested as heuristics for screening candidate lines [9]. Beyond heuristic screening, approximate OTS formulations modify the MIP structure to implicitly penalize switching, enabling near-optimal dispatch while producing much simpler topologies and reducing computation time [10]. Although these methods can yield feasible decisions, they still require

solving numerous OPF or OTS subproblems. These limitations motivate learning-based approaches that aim to better capture the complexity of OTS.

Although learning-based approaches have been explored as an alternative to heuristic OTS methods, there are several challenges. **First**, many learning approaches rely on supervised learning, which requires pre-solved OTS as labels. Obtaining these labels requires repeatedly solving the OTS problem itself, which is computationally expensive and often infeasible for large networks, thereby eliminating the intended advantage of learning-based acceleration. **Second**, end-to-end learning methods that directly predict switching decisions or dispatch values do not enforce power balance, line limits, or generator limits, and can therefore produce infeasible operating points. This is a critical challenge in power system operations, where feasibility violations can lead to insecure or unsafe dispatch outcomes and require operator intervention or fallback procedures. **Third**, existing methods lack adaptability to changes in network constraints. In practical system operations, line flow limits often change due to seasonal conditions or technologies such as dynamic line rating. As a result, models must remain reliable under varying constraint settings to ensure safe and efficient operation.

There have been several efforts in the literature to address these challenges. Specifically, regarding the first challenge, several works have attempted to address the first challenge by adopting reinforcement learning (RL) to learn switching strategies directly from interaction with a simulated grid environment. For example, RL-based OTS methods use DDQN agents to sequentially remove branches without requiring pre-solved optimal solutions [11], and RL agents have been applied to real-time topology control to manage overloads and instability events [12]. RL has also been explored for OTS applications such as short-circuit current mitigation, where DQN agents choose switching actions-based solely on reward feedback rather than labeled OTS data [13]. Although RL removes label dependence, it does not guarantee feasibility. This is because RL agents optimize rewards rather than enforce physical constraints of power system, and can therefore produce infeasible or unsafe switching actions. Thus, feasibility is still not ensured, limiting RL's suitability for OTS.

To address the second challenge, some studies incorporate

feasibility mechanisms during inference. One common approach is to combine learning with optimization by warm starting a solver using predicted switching actions, allowing feasibility to be enforced through a conventional OPF or MILP solver [14]. Other methods apply feasibility checks followed by OPF-based correction steps if the predicted topology leads to constraint violations [15]. However, the performance after post-processing is not guaranteed, as reported in [23]. Furthermore, these methods typically rely on labeled data during training, which involves significant computational overhead in preparing labels. Machine learning approaches for OTS, such as line-ranking and algorithm-selection methods [16], also require labeled optimal switching decisions. Thus, these works do not resolve the first challenge about label dependence.

Although existing methods address either label dependence or feasibility, none explicitly tackle the third challenge. Most prior work evaluates learning models under fixed network constraints, without considering variability in system parameters. As a result, their performance can significantly degrade or remain unchanged when constraint settings change. This lack of adaptability limits their applicability in real system operations, where constraint variability is common [24]. Although learning-based OPF methods have investigated generalization under varying network information [25], [26], no comparable studies have validated this capability in the context of OTS.

In this regard, we propose a dispatch aware deep neural network (DA-DNN) to overcome the aforementioned three challenges of solving OTS. To address the first challenge, DA-DNN is trained in an unsupervised manner using the generation cost from a differentiable DC-OPF layer as the loss function, eliminating the need for labeled OTS solutions. For the second challenge, the DC-OPF layer enforces all physical constraints on dispatch variables during both training and inference. Finally, the third challenge is resolved by incorporating the optimization layer directly into the model. The parameters of the model are updated through implicit differentiation, as commonly adopted in learning-based DC-OPF [23], [27] and AC-OPF [28]. This enables DA-DNN to remain adaptive under changes in network constraints.

This paper builds on our preliminary work in [29] and makes the following key contributions:

- 1) We propose a novel dispatch-aware deep neural network (DA-DNN) to accelerate solving DC-OTS which consists of a line switching layer and a DC-OPF layer. During training, the line switching layer outputs predicted line statuses. Next, the embedded DC-OPF layer solves DC-OPF with these line statuses to obtain the generator dispatch. The resulting generation cost is used as an unsupervised loss, which eliminates the need for precomputed OTS as labels. Since every forward pass solves a DC-OPF, all physical constraints are enforced throughout training and inference. After training, we binarize the relaxed line status and run DC-OPF to obtain a pair of line status and dispatch that is provably feasible. As a result, the total computation time for our method in the inference phase is always equal to that of a single DC-OPF. To the best of our knowledge, this is

the first work that solves DC-OTS in an unsupervised learning method with embedded DC-OPF layer.

- 2) We introduce a weight and bias initialization scheme that ensures that the embedded DC-OPF is feasible from the first iteration. This enables reliable training on large systems, whereas without this initialization the framework fails training, since the DC-OPF repeatedly returns infeasible solutions.
- 3) We evaluate the proposed framework on the IEEE 73,118, and 300 bus systems. The results show that each inference ends in the same computation time as a single DC-OPF solve. Furthermore, in the 300 bus case, a commercial solver fails to complete DC-OTS within days, whereas our framework produces feasible line statuses that reduce generation cost compared to DC-OPF in just milliseconds. Moreover, the proposed method demonstrates strong performance under untrained line flow limits, showing adaptability to changes in network constraints without retraining.

## II. DC OPTIMAL TRANSMISSION SWITCHING MODEL

Suppose that the given power system consists of  $N_b$  buses,  $N_g$  generators, and  $N_l$  lines. Let  $\Xi_{\text{OTS}} := \{\mathbf{p}_g, \boldsymbol{\theta}, \mathbf{z}\}$  be the set of optimization variables, where  $\mathbf{p}_g \in \mathbb{R}^{N_g}$ ,  $\boldsymbol{\theta} \in \mathbb{R}^{N_b}$ , and  $\mathbf{z} \in \{0, 1\}^{N_l}$  denote active power generation, voltage phase angle, and line on/off status. Then, the DC-OTS problem is formulated as follows [30]:

$$\min_{\Xi_{\text{OTS}}} C(\mathbf{p}_g) \quad (1a)$$

$$\mathbf{M}\mathbf{p}_g - \mathbf{p}_d = \mathbf{C}^\top (\mathbf{z} \odot \text{diag}(\mathbf{b}_l)\mathbf{C}\boldsymbol{\theta}), \quad (1b)$$

$$\mathbf{z} \odot \underline{\mathbf{p}}_l \leq \mathbf{z} \odot \text{diag}(\mathbf{b}_l)\mathbf{C}\boldsymbol{\theta} \leq \mathbf{z} \odot \bar{\mathbf{p}}_l, \quad (1c)$$

$$\underline{\mathbf{p}}_g \leq \mathbf{p}_g \leq \bar{\mathbf{p}}_g, \quad (1d)$$

$$\underline{\boldsymbol{\theta}} \leq \boldsymbol{\theta} \leq \bar{\boldsymbol{\theta}}, \quad (1e)$$

$$\theta_{\text{ref}} = 0, \quad (1f)$$

where  $C(\cdot) : \mathbb{R}^{N_g} \rightarrow \mathbb{R}$  in (1a) is the convex generation cost function of each generator. (1b) enforces DC power balance equation, where  $\mathbf{M} \in \{0, 1\}^{N_b \times N_g}$  is generator-bus incidence matrix that maps  $\mathbf{p}_g$  to the vectors of  $N_b$  dimensions,  $\mathbf{p}_d \in \mathbb{R}^{N_b}$  denotes nodal demand of each bus, and  $\mathbf{C}^\top (\mathbf{z} \odot \text{diag}(\mathbf{b}_l)\mathbf{C}\boldsymbol{\theta})$  represents the line flows. Here,  $\mathbf{C} \in \{-1, 0, 1\}^{N_l \times N_b}$  is the branch-bus incidence matrix,  $\mathbf{b}_l \in \mathbb{R}^{N_l}$  is the vector of line susceptances, and  $\odot$  refers to element-wise multiplication. Note that  $\mathbf{z}$  nullifies any line flows that are switched out. These line flows are restricted by  $\underline{\mathbf{p}}_l$  and  $\bar{\mathbf{p}}_l$  in (1c). In addition, the output of the generator and the angle of the nodal voltage are limited by (1d) and (1e), respectively. Finally, (1f) defines the slack bus.

## III. METHODOLOGIES

Unlike DC-OPF, which can be solved in milliseconds, DC-OTS is NP-hard due to the binary vector  $\mathbf{z}$ . Thus, commercial MILP solvers may require several hours or even days to reach optimality. Consequently, practical adoption hinges on accelerated solution techniques. Thus, in this section, we introduce the proposed DA-DNN, an efficient DNN-based

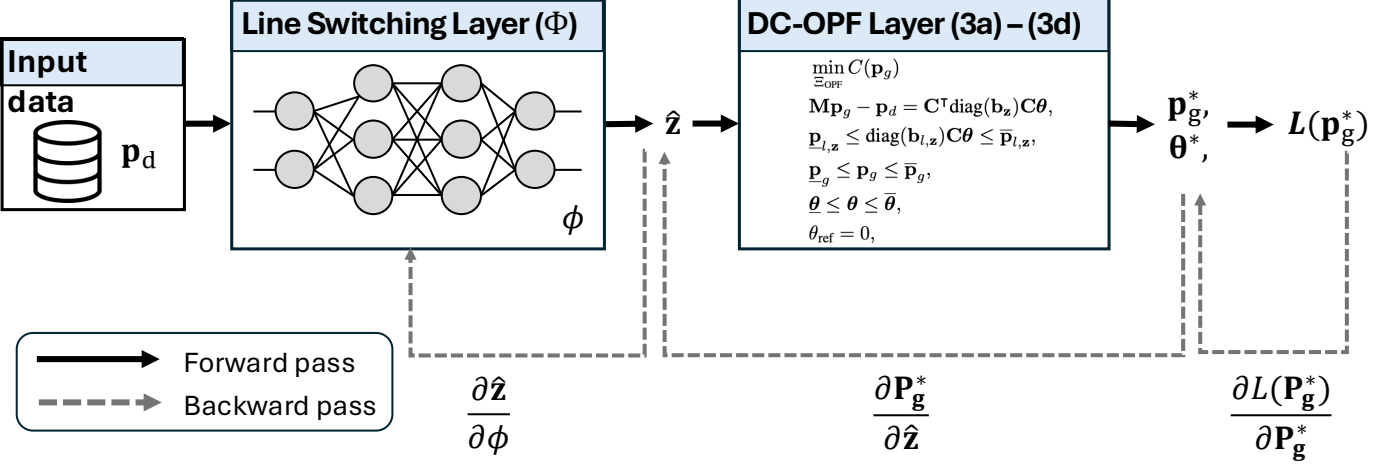


Fig. 1: Training process of the proposed dispatch-aware deep neural network for optimal transmission switching.

method that obtains near-optimal switching decisions within operational time frames.

The overall framework of the proposed DA-DNN is illustrated in Fig. 1. As shown in the figure, DA-DNN consists of a line switching layer and a DC-OPF layer. The line switching layer takes bus demand and predicts the line status of the network. Then, DC-OPF layer takes the predicted line status, solves DC-OPF-based on that values, and obtains dispatch. After that, the model learns to reduce the generation cost that is determined from the obtained dispatch. Note that we don't need to prepare any presolve labes of DC-OTS when training the proposed DA-DNN.

#### A. Forward Pass of DA-DNN

1) *Solving DC-OPF with NN predicted line status:* Let  $\Phi : \mathbb{R}^{N_b} \rightarrow \mathbb{R}^{N_l}$  be the line switching layer in Fig. 1 that maps  $p_d$  to the predicted line switching state  $\hat{z} \in [0, 1]^{N_l}$ , thus we have  $\hat{z} = \Phi(p_d)$ . Note that all elements of  $\hat{z}$  are bounded by  $[0, 1]$ , since  $\hat{z}$  is used as a continuous relaxation of the binary line switch state when solving (3). For this bound, we use a sigmoid function  $\sigma(\cdot)$  as follows:

$$\hat{z} = \sigma(\mathbf{W}^{\text{last}} \tilde{z} + \mathbf{b}^{\text{last}}) \quad (2)$$

where  $\mathbf{W}^{\text{last}} \in \mathbb{R}^{N_h \times N_l}$ ,  $\mathbf{b}^{\text{last}} \in \mathbb{R}^{N_l}$ , and  $\tilde{z}$  are the weight matrix, the bias vector, and the input of the last layer of  $\Phi$ , respectively.

Now, we solve the DC-OPF using  $\hat{z}$ . Let  $\Xi_{\text{OPF}} := \{p_g, \theta\}$  be the set of optimization variables of DC-OPF. Then, the optimization problem is formulated as follows:

$$\min_{\Xi_{\text{OPF}}} C(\mathbf{p}_g) \quad (3a)$$

$$\mathbf{M}\mathbf{p}_g - \mathbf{p}_d = \mathbf{C}^T \text{diag}(\mathbf{b}_{l,z}) \mathbf{C} \theta, \quad (3b)$$

$$\underline{\mathbf{p}}_{l,z} \leq \text{diag}(\mathbf{b}_{l,z}) \mathbf{C} \theta \leq \bar{\mathbf{p}}_{l,z}, \quad (3c)$$

$$(1d) - (1f), \quad (3d)$$

where  $\mathbf{b}_{l,z} = \mathbf{z} \odot \mathbf{b}_l$ ,  $\underline{\mathbf{p}}_{l,z} = \mathbf{z} \odot \underline{\mathbf{p}}_l$ , and  $\bar{\mathbf{p}}_{l,z} = \mathbf{z} \odot \bar{\mathbf{p}}_l$ . This optimization problem is DC-OPF with a continuously relaxed line switching state  $\hat{z}$ .

2) *Weight and bias initialization:* In the initial training process, (3) is likely infeasible, because randomly initialized switching causes arbitrary line status that distort or disconnect the network, causing DC-OPF constraints to be infeasible. Thus, training of the proposed DA-DNN becomes unstable and cannot progress.

Let  $\mathbf{W}_{\text{init}}^{\text{last}}$  and  $\mathbf{b}_{\text{init}}^{\text{last}}$  denote the initial weight matrix and the bias vector of the last layer of  $\Phi$ , respectively. The resulting initial relaxed line state  $\tilde{z}_{\text{init}}$  is

$$\tilde{z}_{\text{init}} = \sigma(\mathbf{W}_{\text{init}}^{\text{last}} \tilde{z}_{\text{init}} + \mathbf{b}_{\text{init}}^{\text{last}}), \quad (4)$$

where  $\tilde{z}_{\text{init}}$  is the input to the last initialized layer. We set  $\mathbf{W}_{\text{init}}^{\text{last}} = \mathbf{0}$  and  $\mathbf{b}_{\text{init}}^{\text{last}} = 9$ , so that every component is evaluated at  $\tilde{z}_{\text{init}} = \sigma(9) = 0.9999$ . Employing  $\tilde{z}_{\text{init}}$  for (3) solves the optimization problem with the standard DC-OPF.

3) *Loss function to train the model:* Let  $\Xi_{\text{OPF}}^* := \{\hat{\mathbf{p}}_g^*, \hat{\theta}^*\}$  be the set of solutions of (3), which is defined as follows:

$$\Xi_{\text{OPF}}^* := \{\hat{\mathbf{p}}_g^*, \hat{\theta}^*\} = \arg \min_{\Xi_{\text{OPF}} \in \mathcal{F}(\hat{z})} C(\mathbf{p}_g) \quad (5)$$

where  $\mathcal{F}(\hat{z})$  is the feasible region determined from  $\hat{z}$ . Now, we determine the loss function using  $\Xi_{\text{OPF}}^*$  to train  $\Phi$  as  $\mathcal{L}(\hat{\mathbf{p}}_g) = C(\hat{\mathbf{p}}_g)$ . Thus, we directly minimize the overall generation cost in an unsupervised learning framework, i.e., we do not need to prepare the presolved solution as labels. In the inference phase, we binarize  $\hat{z}$  based on the threshold (e.g., 0.5), since real-world transmission switching status has only on/off status.

#### B. Backpropagation Through DC-OPF Layer

The backpropagation to train  $\Phi$  with a learnable parameter  $\phi$  (e.g.,  $\mathbf{W}$  and  $\mathbf{b}$ ) is expressed as follows:

$$\nabla_{\phi} \mathcal{L} = \frac{\partial \mathcal{L}}{\partial (\hat{\mathbf{p}}_g^*, \hat{\theta}^*)} \frac{\partial (\hat{\mathbf{p}}_g^*, \hat{\theta}^*)}{\partial \hat{z}} \frac{\partial \hat{z}}{\partial \phi}. \quad (6)$$

Here,  $\frac{\partial \mathcal{L}}{\partial (\hat{\mathbf{p}}_g^*, \hat{\theta}^*)}$  is determined analytically since  $\mathcal{L}(\hat{\mathbf{p}}_g) = C(\hat{\mathbf{p}}_g)$ .  $\frac{\partial \hat{z}}{\partial \phi}$  is determined from automatic differentiation, which is widely adopted to train deep learning models. So,

we need to obtain  $\frac{\partial(\hat{\mathbf{p}}_g^*, \hat{\theta}^*)}{\partial \hat{\mathbf{z}}}$ , which requires derivatives of the argmin function (5).

For this, we simplify the DC-OPF problem (3) as follows:

$$\min_{\mathbf{x}} f(\mathbf{x}) \quad (7a)$$

$$g(\mathbf{x}, \hat{\mathbf{z}}) = 0, \quad (7b)$$

$$h(\mathbf{x}, \hat{\mathbf{z}}) \leq 0, \quad (7c)$$

where  $\mathbf{x}$  denotes the optimization variables of (3). Then, the Lagrange function  $L$  of the optimization problem is formulated as:

$$L(\mathbf{x}, \boldsymbol{\lambda}, \boldsymbol{\mu}; \hat{\mathbf{z}}) = f(\mathbf{x}) + \boldsymbol{\lambda}^\top g(\mathbf{x}, \hat{\mathbf{z}}) + \boldsymbol{\mu}^\top h(\mathbf{x}, \hat{\mathbf{z}}) \quad (8)$$

where  $\boldsymbol{\lambda}$  and  $\boldsymbol{\mu}$  are the dual variables of equality and inequality constraints, respectively. Since (7) is a convex optimization problem, the KKT conditions are sufficient and necessary conditions for optimality. Thus, we have

$$\mathcal{I} := \begin{bmatrix} \frac{\partial L(\mathbf{x}, \boldsymbol{\lambda}, \boldsymbol{\mu}; \hat{\mathbf{z}})}{\partial \mathbf{x}} \\ g(\mathbf{x}, \hat{\mathbf{z}}) \\ h(\mathbf{x}, \hat{\mathbf{z}}) \end{bmatrix} = \mathbf{0} \quad (9)$$

where  $\mathcal{I}$  is the implicit function of  $\mathbf{x}$  and  $\hat{\mathbf{z}}$  for the KKT optimality conditions. Since the derivative of  $\mathcal{I}$  with respect to  $\hat{\mathbf{z}}$  exists due to the implicit function theorem [31], we have

$$\frac{\partial \mathcal{I}}{\partial \hat{\mathbf{z}}} + \frac{\partial \mathcal{I}}{\partial \mathbf{x}} \frac{\partial \mathbf{x}}{\partial \hat{\mathbf{z}}} = \mathbf{0}. \quad (10)$$

Since  $\mathbf{x}$  represents the optimization variables  $\hat{\mathbf{p}}_g^*$  and  $\hat{\theta}^*$ , we have

$$\frac{\partial(\hat{\mathbf{p}}_g^*, \hat{\theta}^*)}{\partial \hat{\mathbf{z}}} = - \left( \frac{\partial \mathcal{I}}{\partial(\hat{\mathbf{p}}_g^*, \hat{\theta}^*)} \right)^{-1} \frac{\partial \mathcal{I}}{\partial \hat{\mathbf{z}}}. \quad (11)$$

It should be noted that  $\frac{\partial \mathcal{I}}{\partial \hat{\mathbf{z}}}$  and  $\frac{\partial \mathcal{I}}{\partial \mathbf{x}}$  are both explicitly determined. Hence, we now have the backpropagation process to update  $\phi$  of  $\Phi$  as follows:

$$\nabla_\phi \mathcal{L} = - \frac{\partial \mathcal{L}}{\partial(\hat{\mathbf{p}}_g^*, \hat{\theta}^*)} \left( \frac{\partial \mathcal{I}}{\partial(\hat{\mathbf{p}}_g^*, \hat{\theta}^*)} \right)^{-1} \frac{\partial \mathcal{I}}{\partial \hat{\mathbf{z}}} \frac{\partial \hat{\mathbf{z}}}{\partial \phi}. \quad (12)$$

Using this result, the learnable parameter  $\phi$  is updated as follows:

$$\phi \leftarrow \phi + \eta_{lr} \frac{\partial \mathcal{L}}{\partial(\hat{\mathbf{p}}_g^*, \hat{\theta}^*)} \left( \frac{\partial \mathcal{I}}{\partial(\hat{\mathbf{p}}_g^*, \hat{\theta}^*)} \right)^{-1} \frac{\partial \mathcal{I}}{\partial \hat{\mathbf{z}}} \frac{\partial \hat{\mathbf{z}}}{\partial \phi} \quad (13)$$

where  $\eta_{lr}$  denotes the learning rate of DA-DNN. We provide pseudo-code for the training process of the proposed method in Algorithm 1.

### C. Inference Process of DA-DNN

In the inference phase, DA-DNN uses binarized line-status decisions rather than the continuous relaxed outputs used during training. Given a load vector, the model first produces the relaxed switching vector  $\hat{\mathbf{z}} = [\hat{z}_\ell]_{\ell=1}^{N_\ell} \in [0, 1]^{N_\ell}$ , which is converted into a binary topology by applying a fixed threshold:

$$\bar{z}_\ell = B(\hat{z}_\ell) = \begin{cases} 1, & \hat{z}_\ell \geq 0.5, \\ 0, & \hat{z}_\ell < 0.5, \end{cases} \quad (14)$$

---

### Algorithm 1 Training process of DA-DNN

---

1: **Inputs:**  
 Training dataset  $\mathcal{D} = \{\mathbf{p}_d^{(n)}\}_{n=1}^N$ ,  
 Learning rate  $\eta_{lr}$ ,  
 Maximum training epochs  $T$ ,  
 Initial parameters  $(\mathbf{W}, \mathbf{b})$ ,  
 DC-OPF solver  $\mathcal{S}_{\text{OPF}}(\cdot)$

2: **Initialize:**  
 Set  $\mathbf{W}$  and  $\mathbf{b}$  randomly,  
 Set  $\mathbf{W}_{\text{last}}^{\text{init}} = \mathbf{0}$ ,  $\mathbf{b}_{\text{last}}^{\text{init}} = 9$

3: **for**  $t \in \{1, \dots, T\}$  **do**

4:   **for all**  $\mathbf{p}_d \in \mathcal{D}$  **do**

5:     **Forward pass:**

6:        $\hat{\mathbf{z}} = f_\phi(\mathbf{p}_d)$  // line switching layer

7:        $(\hat{\mathbf{p}}_g^*, \hat{\theta}^*) \leftarrow \mathcal{S}_{\text{OPF}}(\hat{\mathbf{z}}, \mathbf{p}_d)$  // Solve DC-OPF using  $\hat{\mathbf{z}}$

8:        $\mathcal{L} = C(\hat{\mathbf{p}}_g^*)$  // Compute loss function

9:     **Backward pass:**

10:      $\nabla_\phi \mathcal{L} = - \frac{\partial \mathcal{L}}{\partial(\hat{\mathbf{p}}_g^*, \hat{\theta}^*)} \left( \frac{\partial \mathcal{I}}{\partial(\hat{\mathbf{p}}_g^*, \hat{\theta}^*)} \right)^{-1} \frac{\partial \mathcal{I}}{\partial \hat{\mathbf{z}}} \frac{\partial \hat{\mathbf{z}}}{\partial \phi}$

11:     Update parameters:  $\phi \leftarrow \phi - \eta_{lr} \nabla_\phi \mathcal{L}$

12:   **end for**

13: **end for**

14: **Output:**  $\phi^*$

---



---

### Algorithm 2 Inference process of DA-DNN

---

1: **Inputs:**  
 Trained parameters  $\phi^* = (\mathbf{W}^*, \mathbf{b}^*)$ ,  
 DC-OPF solver  $\mathcal{S}_{\text{OPF}}(\cdot)$ ,  
 Inference dataset  $\mathcal{D}_{\text{inf}} = \{\mathbf{p}_d^{(n)}\}_{n=1}^{N_{\text{inf}}}$ ,  
 Binarization function  $B(\cdot)$

2: **Initialize:**  
 Set  $\phi \leftarrow \phi^*$

3: **for all**  $\mathbf{p}_d \in \mathcal{D}_{\text{inf}}$  **do**

4:   **Forward pass:**

5:      $\hat{\mathbf{z}} = f_\phi(\mathbf{p}_d)$  // output of previous layers

6:      $\bar{\mathbf{z}} \leftarrow B(\hat{\mathbf{z}})$  // Binarization

7:     **Solve DC-OPF under predicted topology:**

8:      $(\hat{\mathbf{p}}_g^*, \hat{\theta}^*) \leftarrow \mathcal{S}_{\text{OPF}}(\bar{\mathbf{z}}, \mathbf{p}_d)$

9:     Store  $(\mathbf{p}_d, \bar{\mathbf{z}}, \hat{\mathbf{p}}_g^*, \hat{\theta}^*)$

10: **end for**

11: **Output:** A set of  $(\mathbf{p}_d, \bar{\mathbf{z}}, \hat{\mathbf{p}}_g^*, \hat{\theta}^*)$ .

---

where  $\bar{\mathbf{z}} = [\bar{z}_\ell]_{\ell=1}^{N_\ell} \in \{0, 1\}^{N_\ell}$ . A single DC-OPF is then solved under this fixed topology to obtain the final dispatch by solving the following optimization problems:

$$\min_{\mathbf{x}} f(\mathbf{x}) \quad (15a)$$

$$g(\mathbf{x}, \bar{\mathbf{z}}) = 0, \quad (15b)$$

$$h(\mathbf{x}, \bar{\mathbf{z}}) \leq 0, . \quad (15c)$$

The inference procedure is summarized in Algorithm 2.

#### IV. CASE STUDY

##### A. Test Systems and Data Generation

We evaluate the proposed DA-DNN on test systems from the PGLib-OPF library [32]. We consider the IEEE 73, 118, and 300 bus systems for evaluation.

For each test system, we generate a dataset of load snapshots by uniformly scaling the base-case demands. Let  $\mathbf{p}_d^{\text{base}} \in \mathbb{R}^{N_b}$  denote the nominal bus demands from PGLib. For each data  $n$ , we draw a scalar factor  $\alpha^{(n)} = [\alpha_i^{(n)}]_{i=1}^{N_b}$  where  $\alpha_i^{(n)} \sim \mathcal{U}(1.00, 1.10)$  and construct

$$\mathbf{p}_d^{(n)} = \alpha^{(n)} \mathbf{p}_d^{\text{base}}, \quad (16)$$

as done in [33]. In this way, each scenario corresponds to a different system-wide loading level between 100% and 110% of the base case. Generator cost coefficients, capacity limits, and line limits are determined from the corresponding PGLib test system. Voltage angle limits are set to 0.6 [1], [22].

For each network, we generate load data by repeatedly sampling the loading factor and solving the corresponding DC-OPF. We retain only scenarios that are at least feasible for DC-OPF and continue this process until we obtain 3,000 feasible load data. These 3,000 scenarios constitute the dataset used for training and evaluation of all learning-based methods.

For each data, the feasible load snapshots are randomly partitioned into three disjoint sets: 50% for training, 16.7% for validation, and 33.3% for testing. The validation set is used for hyperparameter selection, while all performance metrics reported in Section IV are computed on the test set. The same train/validation/test split is used for all learning-based methods to ensure a fair comparison.

##### B. Baselines and implementations details

1) **Baselines:** As illustrated in Fig. 2, we compare the proposed DA-DNN against both conventional optimization baselines and learning-based approaches:

- **ED (Economic Dispatch; Gurobi):** A baseline that ignores all network constraints and optimizes only the generation cost subject to generator limits. ED problem is solved using Gurobi, and its solution provides a theoretical lower bound on the operating cost.
- **DC-OPF (Gurobi):** The DC-OPF formulation solved by the commercial solver Gurobi [34]. DC-OPF is solved as a convex quadratic program and represents the cost of operating the grid without topology control.
- **DC-OTS (Gurobi):** The mixed-integer DC-OTS formulation solved by the commercial solver Gurobi [34]. We impose a time limit of two days per instance and leave all other parameters at their default values unless otherwise stated. When the solver converges within the time limit, DC-OTS provides a globally optimal benchmark for the given loading scenario.
- **SL (Supervised Learning):** The supervised model first predicts the binary line-status vector  $\mathbf{z} \in \{0, 1\}^{N_e}$  from the load vector  $\mathbf{p}_d$ , as done in [15]. Given the predicted topology, DC-OPF problem is solved to obtain the final dispatch ( $\mathbf{p}_g, \theta$ ), which is consistent with [35]. This

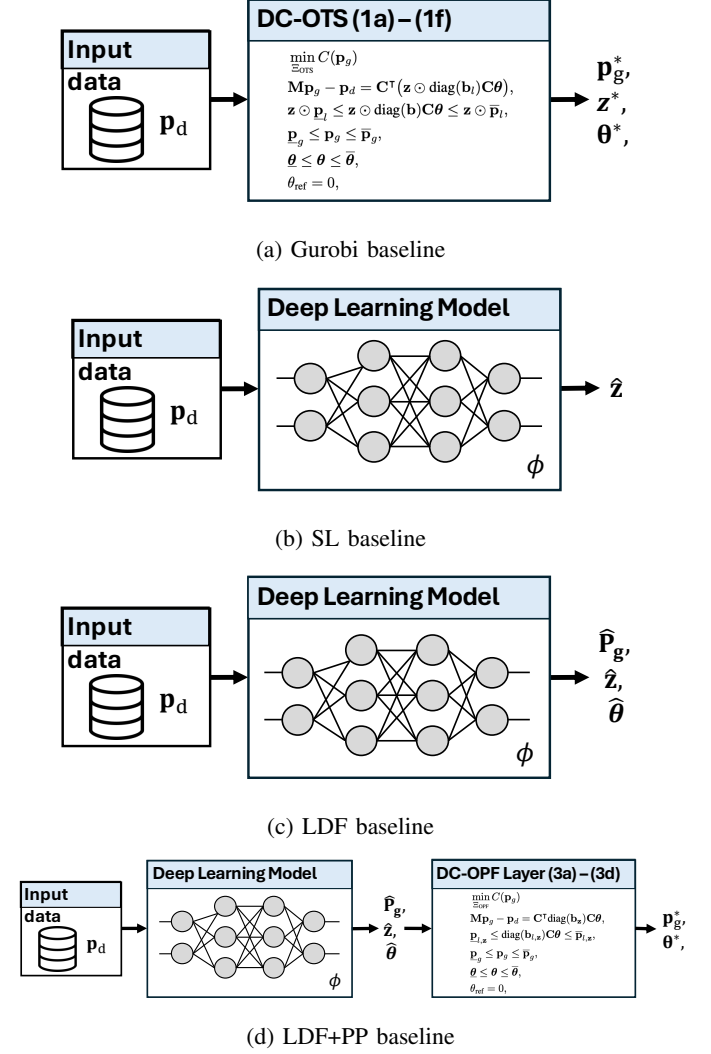


Fig. 2: DC-OTS baseline comparisons

approach evaluates whether feasibility can be recovered by projecting NN-predicted switching decisions onto the OPF feasible set. As with SL, this method is applicable only when sufficient OTS labels are available for training.

- **LDF (Lagrange-Dual Formulation):** An unsupervised model that maps the load vector  $\mathbf{p}_d$  directly to  $\mathbf{p}_g$ ,  $\theta$ , and  $\mathbf{z}$ . The model is trained to minimize the lagrange function without explicitly enforcing power balance, generator limits, or line-flow constraints, as done in [36]. Since no OPF layer is embedded, the predicted operating point may violate multiple physical constraints and result in infeasible solutions.
- **LDF+PP (LDF + Post-Processing):** The LDF model is used to obtain the line-status  $\mathbf{z}$ . After that, a single DC-OPF is solved to obtain the corresponding generator dispatch and voltage angles. This baseline evaluates whether feasible operating points can be recovered by solving DC-OPF under the predicted line status, even though the LDF model itself does not explicitly enforce physical constraints.

- 2) **Implementation Details:** All neural models are implemented in PyTorch. We use a three layers of fully connected

TABLE II. OVERALL PERFORMANCE COMPARISON IN IEEE 73 AND 118 BUS SYSTEMS.

Problem	Method	IEEE 73 bus system				IEEE 118 bus system			
		Avg. gen. cost (\$1k)	Avg. ineq. viol. (%)	Avg. eq. viol. (%)	Avg. comp. time (sec)	Avg. gen. cost (\$1k)	Avg. ineq. viol. (%)	Avg. eq. viol. (%)	Avg. comp. time (sec)
ED	Gurobi	183.01	0.00	0.00	0.00 $\pm$ 0.00	93.01	0.00	0.00	0.00 $\pm$ 0.00
DC-OPF	Gurobi	183.01	0.00	0.00	0.00 $\pm$ 0.00	93.16	0.00	0.00	0.00 $\pm$ 0.00
DC-OTS	Gurobi	183.01	0.00	0.00	1.85 $\pm$ 1.35	93.01	0.00	0.00	19.14 $\pm$ 199.44
	SL	183.01	0.00	0.00	0.00 $\pm$ 0.00	93.03	0.00	0.00	0.00 $\pm$ 0.00
	LDF	152.03	100.00	100.00	0.00 $\pm$ 0.00	29.48	100.00	100.00	0.00 $\pm$ 0.00
	LDF+PP	-	100.00	100.00	-	100.00	100.00	-	-
<b>DA-DNN (Proposed)</b>		183.01	0.00	0.00	0.00 $\pm$ 0.00	93.03	0.00	0.00	0.00 $\pm$ 0.00

neural network for the line-switching layer. The hidden dimension is set to 128 for the IEEE 73 bus system and IEEE 118 bus system, and 256 for the IEEE 300 bus system. We employ the exponential linear unit (ELU) as the activation function for all hidden layers [37], dropout rate of 0.1 [38], and a sigmoid activation for the final line-status output layer of DA-DNN to ensure  $\hat{\mathbf{z}} \in [0, 1]^{N_e}$ .

The neural network baselines (SL, LDF, and LDF+PP) and the proposed DA-DNN are trained using the AdamW optimizer [39] with a learning rate of  $5 \times 10^{-5}$  and a weight decay of  $10^{-2}$ . We use a mini-batch size of 50 and train for up to 40 epochs. The DC-OPF layer in DA-DNN is implemented via CVXPYLayer [40] and solved with the Clarabel solver [41] for training. For inference phase, all methods solving the optimization problem (ED, DC-OPF, DC-OTS, SL, LDF+PP, DA-DNN) use Gurobi solver [34] with two days of time limit using 64 threads, and a MIP gap of  $10^{-5}$ .

### C. Overall Performance Comparisons

The overall performance comparisons are summarized in Table II. We start our discussion with the IEEE 73 bus system, which represents a non-binding operating regime. In this case, ED, DC-OPF, and DC-OTS yield identical generation costs across all tested load scenarios, indicating that network constraints are largely non-binding even under varying load levels. Consequently, transmission switching does not provide additional economic benefits in this system. Importantly, the proposed DA-DNN correctly follows DC-OPF and DC-OTS solutions without introducing unnecessary switching actions. This behavior is desirable from an operational perspective, as it confirms that DA-DNN does not induce unnecessary topology changes in uncongested systems.

In contrast, learning-based baselines exhibit fundamentally different behavior in this non-binding regime. In particular, LDF produces extremely low numerical generation costs (e.g., 152.03k), but these values are entirely meaningless because the predicted solutions violate both equality and inequality constraints by 100%. Even when post-processing is applied (LDF+PP), the predicted line-status configurations frequently lead to infeasible DC-OPF problems, resulting in complete constraint violations. These results highlight that, even in a non-binding system where the optimal solution is trivial, physics-unaware learning approaches fail to produce valid operating points, underscoring the necessity of embedding power system constraints into the learning framework.

We next consider the IEEE 118 bus system, where network constraints become binding and transmission switching provides tangible economic benefits. In this case, DA-DNN yields an average generation cost of 93.03k, compared to the optimal DC-OTS cost of 93.01k, which corresponds to an optimality gap of 0.02%. Although this gap is not exactly zero, the difference in cost is very small. In contrast, the difference in computational time is substantial. For example, the Gurobi-based mixed-integer OTS solver requires 19.14  $\pm$  199.44 seconds, and the large standard deviation indicates that the computation time can vary widely across instances. This variability is challenging for real-time operations, where reliable and consistent computation is essential for both dispatch and corrective switching [42].

In contrast, learning-based approaches offer consistent and system-independent computation time, since inference consists of a single neural network forward pass followed by one DC-OPF solve. Among them, DA-DNN is the most efficient: it produces a feasible topology-dispatch pair in the time of a single DC-OPF solve, with negligible variance across all test scenarios. Moreover, it guarantees feasibility at every step by embedding the OPF layer directly into training and inference. Although SL shows a similar average cost in the 118 bus system, this result is misleading from an operational perspective. This is because SL requires pre-solved OTS labels, which necessitates solving thousands of mixed-integer programs offline using conventional solvers. This limitation increases the overall computational burden and prevents SL from serving as a practical real-time OTS method, particularly when operating conditions or network constraints change.

Overall, DA-DNN achieves near-optimal OTS performance when transmission switching is beneficial, matches the DC-OPF solution in uncongested systems, and provides strict feasibility and real-time computation without requiring labeled OTS data. This combination of economic efficiency, computational stability, and operational reliability makes the proposed method well-suited for deployment in real-time OTS.

### D. Overall Performance Comparisons in 300 bus system

The results for the IEEE 300 bus system are summarized in Table III. This case represents a larger network where DC-OTS formulation becomes difficult to solve. For the full dataset, Gurobi fails to obtain a global optimal solution within the 48-hour time limit, underscoring the well-known scalability limitations of OTS in large transmission networks. As a result,

TABLE III. OVERALL PERFORMANCE COMPARISON ON IEEE 300 BUS SYSTEMS. THE COLUMN WITH DATASET REFER TO THE RESULTS WITH ENTIRE GENERATED DATASET, WHILE SINGLE REFER TO THE RESULTS FROM SINGLE LOAD PROFILE PROVIDED IN PGLIB.

Problem	Method	IEEE 300 bus system (dataset)				IEEE 300 bus system (single)			
		Avg. gen. cost (\$1k)	Avg. ineq. viol. (%)	Avg. eq. viol. (%)	Avg. comp. time (sec)	Avg. gen. cost (\$1k)	Avg. ineq. viol. (%)	Avg. eq. viol. (%)	Avg. comp. time (sec)
ED	Gurobi	481.00	0.00	0.00	0.00±0.00	481.05	0.00	0.00	0.00
DC-OPF	Gurobi	524.52	0.00	0.00	0.01±0.00	524.00	0.00	0.00	0.01
DC-OTS	Gurobi	-	-	-	NS.	515.94	-	-	51.00*
	SL	-	-	-	-	-	-	-	-
	LDF	332.39	100.00	100.00	0.00±0.00	277.17	100.00	100.00	0.00
	LDF+PP	-	100.00	100.00	-	-	100.00	100.00	-
<b>DA-DNN (Proposed)</b>		516.37	0.00	0.00	0.01±0.00	515.94	0.00	0.00	0.01

NS.: not solved within 48 hours. \* indicate the computation time when Gurobi reaches DA-DNN's generation cost

SL baseline, which requires optimal OTS labels, cannot be applied in this system.

On the full dataset of 3,000 load scenarios, the remaining learning-based baselines also show poor performance. LDF produces extremely low numerical generation costs, but these values arise solely from unconstrained outputs and correspond to 100% % of equality and inequality violations, making them physically meaningless. LDF+PP simply solves a DC-OPF using the line status predicted by LDF; however, because these predicted topologies are physically invalid, the resulting operating points also exhibit 100% constraint violations. In contrast, the proposed DA-DNN maintains strict feasibility across all dataset scenarios and achieves an average generation cost of 516.37k, which is 1.55% lower than the DC-OPF. Since DA-DNN requires approximately 0.01 seconds for inference, it is the only method in Table III that reliably obtain feasible solutions to this large-scale system while providing meaningful benefits of solving OTS.

A more detailed comparison is obtained from the single PGLib load profile. In this case, we do not use Gurobi to obtain a globally optimal OTS solution, since the solver does not converge within the time limit. Instead, we monitor the variation of the incumbent objective value and record the computation time at which Gurobi first reaches a generation cost equal to that of DA-DNN (515.94k). The value reported in Table III (marked with \*) therefore represents the time required for Gurobi to match the DA-DNN cost, which is approximately 51 seconds in this case, as illustrated in Fig. 3. Note that DA-DNN achieves its final cost within 0.01 sec, but its curve is drawn horizontally in Fig. 3 only to visually compare against the much slower convergence of Gurobi.

These results show that DA-DNN is the only method capable of producing feasible, high-quality, and economically meaningful switching solutions on the 300 bus network among the methods in Table III. Although Gurobi and other learning-based baselines become unusable due to infeasibility, reliance on unavailable labels, or excessive computation, DA-DNN preserves scalability and real-time capability, demonstrating its practicality for solving OTS in large transmission systems.

#### E. Inference with Untrained Line Flow Limits

As described in Section IV-A, the proposed DA-DNN is trained under the nominal static line ratings (SLR) corresponding to 100% of line flow limits. However, in practical

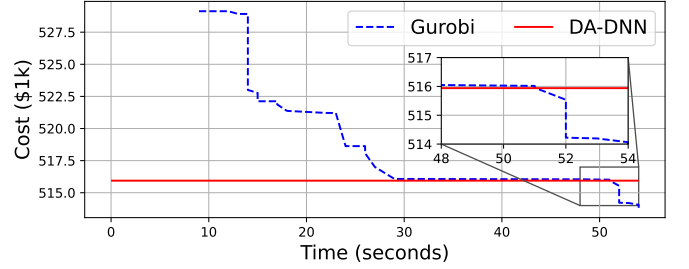


Fig. 3: Generation cost trajectories of Gurobi for solving DC-OTS of the IEEE 300 bus single case. DA-DNN achieves its final cost within 0.01 sec (see Table III), and its line is shown horizontally only for visual comparison.

TABLE IV. GENERATION COST UNDER UNTRAINED LINE LIMITS. THE LEARNING-BASED METHODS ARE TRAINED ON 100% OF LINE LIMITS.

Line limit (%)	Average generation cost (\$1k)				
	ED		DC-OPF		
	Gurobi	Gurobi	Gurobi	LDF	DA-DNN
90	93.01	93.78	93.02	29.48	93.34
95	93.01	93.32	93.02	29.48	93.13
100	93.01	93.16	93.01	29.48	93.03
110	93.01	93.03	93.01	29.48	93.01
120	93.01	93.01	93.01	29.48	93.01
130	93.01	93.01	93.01	29.48	93.01

grids, transmission capacities often deviate from their static values due to ambient conditions, seasonal variations, and the deployment of dynamic line ratings (DLRs). In most real-world DLR applications, these dynamically determined line flow limits are higher than the SLRs, while cases where DLR falls below the SLR occur much less frequently [43].

To examine this practical scenario, we evaluate the generation cost of Gurobi-based and unsupervised learning method under a wide range of untrained line flow limits between 90% and 130%. As shown in Table IV and Fig. 4, DA-DNN closely tracks the behavior of DC-OPF and DC-OTS as line flow limits vary. For higher limits, which correspond to conditions commonly observed in DLR-enabled systems, the proposed model automatically adapts to the expanded feasible region and achieves costs nearly identical to the optimal OTS solution. This adaptability arises because the embedded differentiable DC-OPF layer enforces physical constraints using the actual line-flow limits provided at inference

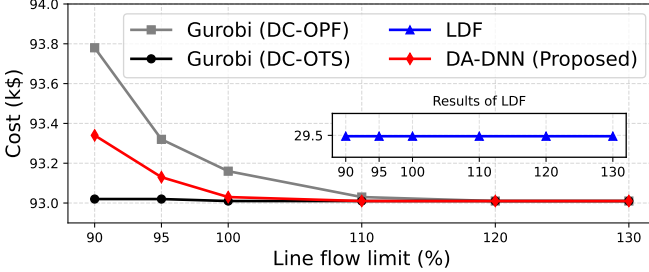


Fig. 4: Generation cost comparisons with varying line flow limits.

time. As a result, DA-DNN does not need to learn explicit mappings for every possible constraint configuration; instead, the OPF layer recalculates feasible dispatch decisions for any new operating condition. This mechanism enables strong generalization to environments that the model has never seen during training. In contrast, the LDF method outputs the same value across all limit settings because it directly maps the load vector to dispatch without incorporating network constraints. Consequently, LDF cannot respond to changes in line flow limits and completely fails in environments that differ from the trained system configuration.

When line flow limits are more restrictive than those used during training, DA-DNN shows a moderate increase in generation cost, which is expected due to the reduced feasible region. Moreover, DA-DNN remains feasible in all cases and maintains costs lower than the DC-OPF benchmark. These results indicate that the proposed method not only performs well under nominal conditions but also maintains reliability and economic efficiency across a wide range of realistic operating environments, including those encountered in systems with DLRs.

#### F. Impact of the weight and-bias initialization

From now on, we focus on analyzing the impact of the employed weight-bias initialization. Fig. 5 shows the histogram of the relaxed line status values produced by an untrained DA-DNN under two different initializations. With the proposed manual methodology, almost every value is 0.9999, which corresponds to zero off line state topology. In contrast, a standard random initialization scatters the output throughout the  $[0, 1]$  range. Since we prepare dataset that are feasible in DC-OPF, the all-closed topology is always feasible. Thus, the manual initialization guarantees that the very first forward pass can be trained through the embedded DC-OPF, whereas the random approach leads to infeasible OPF and blocks the learning process.

Fig. 6 shows the resulting training curves for the IEEE 73, 118, and 300 bus systems. At epoch 0, the embedded optimization problem coincides with the DC-OPF benchmark because all line-status values are initialized close to 1. This guarantees a feasible operating point at the start of training, allowing gradients to propagate properly through the OPF layer. The generation cost then decreases smoothly without instability. In contrast, with random weight initialization, the relaxed switching values  $\hat{z}$  are scattered across the entire  $[0, 1]$

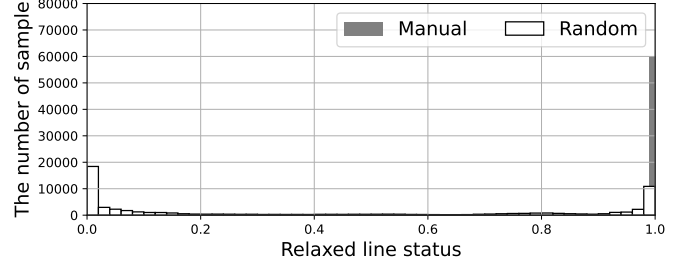


Fig. 5: Histogram of the predicted relaxed line status values from untrained DA-DNN with different weight and bias initialization.

range, as shown in Fig. 5. This results in arbitrary partial line openings in the first iteration, which often makes the embedded DC-OPF layer infeasible. Once the OPF fails, gradients cannot be computed, and the network is unable to make meaningful updates. As a result, training does not progress and the loss remains unchanged.

These observations demonstrate that the proposed manual weight-bias initialization is essential for stable learning of OTS. By ensuring that the first forward pass always yields a feasible DC-OPF solution, initialization enables valid gradients to flow through the OPF layer from the beginning of training. This provides a well-conditioned starting point from which the network can gradually adjust line statuses and learn a cost-reducing switching policy while satisfying all physical constraints throughout the entire training process.

## V. CONCLUSION

In this paper, we proposed a dispatch-aware deep neural network (DA-DNN) consisting of a line-switching layer and an embedded differentiable DC-OPF layer. This design enables fully unsupervised training while guaranteeing feasibility at every training step and during inference. In addition, a customized weight-bias initialization ensures that learning begins from a valid operating point, even for large networks. Once trained, DA-DNN produces a topology-dispatch pair within the computation time of a single DC-OPF solve while achieving the economic benefits of DC-OTS. Simulation results on the IEEE 73, 118, and 300 bus systems demonstrated that DA-DNN consistently lowers generation cost compared to DC-OPF, and much faster than conventional solver in solving DC-OTS. Notably, commercial solvers fail to solve the DC-OTS problem within two days on the 300 bus system, whereas DA-DNN computes feasible switching actions in milliseconds, underscoring its scalability and real-time suitability. Furthermore, even in the varying line flow limits, DA-DNN maintains feasibility and lower generation cost than DC-OPF across a wide range of untrained line flow limits without retraining, which demonstrates DA-DNN's high generalization ability.

For future work, we plan to extend the framework in three directions. First, we will replace the DC-OPF layer with an AC-OPF layer and incorporate security constraints. Second, we plan to develop a multi-step switching schedules under forecast uncertainty in load, renewables, and contingencies. Lastly, we will incorporate the stability constraints for the applicability of the real-world OTS problem.

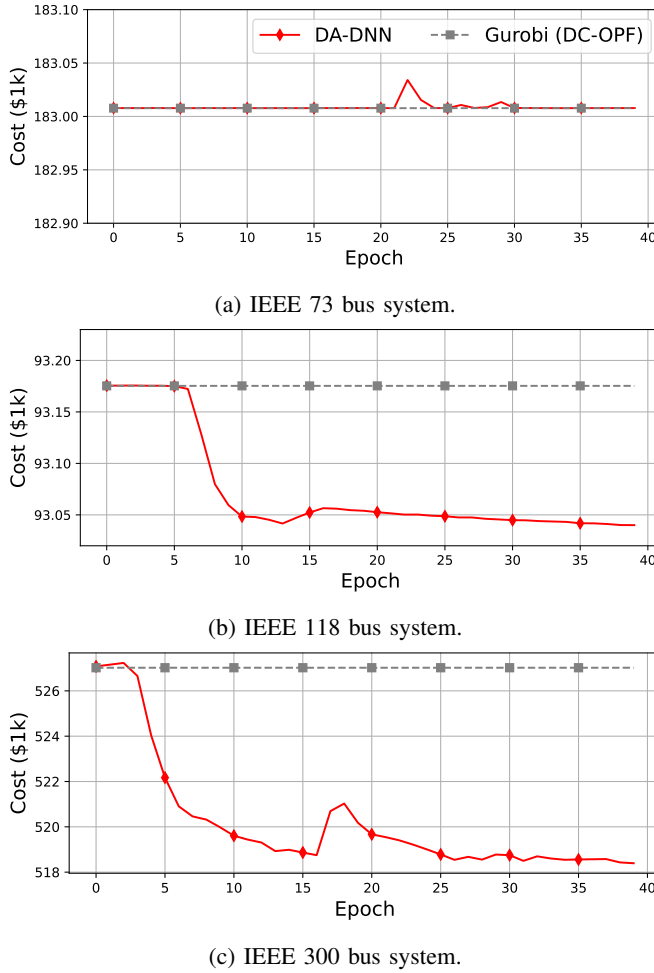


Fig. 6: Training loss curve in various test system.

## REFERENCES

- [1] E. B. Fisher *et al.*, “Optimal transmission switching,” *IEEE transactions on power systems*, vol. 23, no. 3, pp. 1346–1355, 2008.
- [2] B. Schäfer, T. Pesch, D. Manik, J. Gollenstede, G. Lin, H.-P. Beck, D. Withaut, and M. Timme, “Understanding Braess’ paradox in power grids,” *Nature Communications*, vol. 13, no. 1, p. 5396, 2022.
- [3] P. A. Ruiz. (2014) Topology Control Algorithms Project Experience. ARPA-E.
- [4] P. Ruiz, J. Caspary, and L. Butler, “Transmission Topology Optimization Case Studies in SPP and ERCOT,” Presentation at the FERC Technical Conference on Increasing Day-Ahead and Real-Time Market Efficiency and Enhancing Resilience through Improved Software.
- [5] P. Ruiz and M. Myhre, “Congestion Mitigation with Transmission Reconfigurations,” Presentation at the Organization of MISO States Market and Transmission Work Groups Meeting.
- [6] P. A. Ruiz, J. M. Foster, A. Rudkevich, and M. C. Caramanis, “Tractable transmission topology control using sensitivity analysis,” *IEEE Transactions on Power Systems*, vol. 27, no. 3, pp. 1550–1559, 2012.
- [7] J. D. Fuller *et al.*, “Fast heuristics for transmission-line switching,” *IEEE Transactions on Power Systems*, vol. 27, no. 3, pp. 1377–1386, 2012.
- [8] K. W. Hedman, R. P. O’Neill, E. B. Fisher, and S. S. Oren, “Optimal transmission switching with contingency analysis,” *IEEE Transactions on Power Systems*, vol. 24, no. 3, pp. 1577–1586, 2009.
- [9] C. Barrows *et al.*, “Using network metrics to achieve computationally efficient optimal transmission switching,” in *2013 46th Hawaii International Conference on System Sciences*. IEEE, 2013, pp. 2187–2196.
- [10] M. Jabarnejad, “Approximate optimal transmission switching,” *Electric Power Systems Research*, vol. 161, pp. 1–7, 2018.
- [11] T. Han and D. J. Hill, “Learning-based topology optimization of power networks,” *IEEE Transactions on Power Systems*, 2022.
- [12] M. Lehna *et al.*, “Managing power grids through topology actions: A comparative study between advanced rule-based and reinforcement learning agents,” *Energy and AI*, vol. 14, p. 100276, 2023.
- [13] S. Tang *et al.*, “Optimal transmission switching for short-circuit current limitation based on deep reinforcement learning,” *Energies*, 2022.
- [14] S. Pineda *et al.*, “Learning-assisted optimization for transmission switching,” *Top*, vol. 32, no. 3, pp. 489–516, 2024.
- [15] A.-A. B. Bugaje, J. L. Cremer, and G. Strbac, “Real-time transmission switching with neural networks,” *IET Generation, Transmission & Distribution*, vol. 17, no. 3, pp. 696–705, 2023.
- [16] Z. Yang and S. Oren, “Line selection and algorithm selection for transmission switching by machine learning methods,” in *2019 IEEE Milan PowerTech*. IEEE, 2019, pp. 1–6.
- [17] Federal Energy Regulatory Commission. (2025) Explainer on transmission planning and cost allocation final rule. Federal Register.
- [18] ENTSO-E. (2016) Entso-e roadmap 2017-2026. ENTSO-E.
- [19] PJM, *PJM Manual 37: Reliability Coordination*, PJM, 2021.
- [20] I. N. England, *ISO New England Operating Procedure No. 19: Transmission Operations*, ISO New England, 2021.
- [21] M. Numan *et al.*, “The role of optimal transmission switching in enhancing grid flexibility: A review,” *IEEE Access*, vol. 11, 2023.
- [22] C. Crozier *et al.*, “Feasible region-based heuristics for optimal transmission switching,” *Sustainable Energy, Grids and Networks*, 2022.
- [23] M. Kim and H. Kim, “Projection-aware deep neural network for DC optimal power flow without constraint violations,” in *2022 IEEE International Conference on Communications, Control, and Computing Technologies for Smart Grids (SmartGridComm)*. IEEE, 2022.
- [24] C. J. Wallnerström *et al.*, “Impact from dynamic line rating on wind power integration,” *IEEE Transactions on Smart Grid*, 2014.
- [25] Y. Chen *et al.*, “A meta-learning approach to the optimal power flow problem under topology reconfigurations,” *IEEE Open Access Journal of Power and Energy*, vol. 9, pp. 109–120, 2022.
- [26] S. Liu, C. Wu, and H. Zhu, “Topology-aware graph neural networks for learning feasible and adaptive AC-OPF solutions,” *IEEE Transactions on Power Systems*, vol. 38, no. 6, pp. 5660–5670, 2022.
- [27] Y. Kim *et al.*, “MPA-DNN: Projection-Aware Unsupervised Learning for Multi-period DC-OPF,” *arXiv preprint arXiv:2510.09349*, 2025.
- [28] M. Kim and H. Kim, “Unsupervised deep lagrange dual with equation embedding for ac optimal power flow,” *IEEE Transactions on Power Systems*, vol. 40, no. 1, pp. 1078–1090, 2024.
- [29] M. Kim and J. Kim, “Dispatch-Aware Deep Neural Network for Optimal Transmission Switching: Toward Real-Time and Feasibility Guaranteed Operation,” *arXiv preprint arXiv:2507.17194*, 2025.
- [30] A. Ahmadi *et al.*, “Decomposition-Based Stacked Bagging Boosting Ensemble for Dynamic Line Rating Forecasting,” *IEEE Transactions on Power Delivery*, vol. 38, no. 5, pp. 2987–2997, 2023.
- [31] S. G. Krantz and H. R. Parks, *The implicit function theorem: history, theory, and applications*. Springer Science & Business Media, 2002.
- [32] S. Babaeinejad sarookolaei *et al.*, “The power grid library for benchmarking ac optimal power flow algorithms,” *arXiv preprint arXiv:1908.02788*, 2019.
- [33] A. S. Zamzam and K. Baker, “Learning optimal solutions for extremely fast AC optimal power flow,” in *2020 IEEE international conference on communications, control, and computing technologies for smart grids (SmartGridComm)*. IEEE, 2020, pp. 1–6.
- [34] Gurobi Optimization, LLC, “Gurobi Optimizer Reference Manual,” 2024. [Online]. Available: <https://www.gurobi.com>
- [35] X. Pan, T. Zhao, M. Chen, and S. Zhang, “Deepopf: A deep neural network approach for security-constrained dc optimal power flow,” *IEEE Transactions on Power Systems*, vol. 36, no. 3, pp. 1725–1735, 2020.
- [36] F. Fioretto *et al.*, “Lagrangian duality for constrained deep learning,” in *Joint European conference on machine learning and knowledge discovery in databases*. Springer, 2020, pp. 118–135.
- [37] D.-A. Clevert, T. Unterthiner, and S. Hochreiter, “Fast and accurate deep network learning by exponential linear units (elus),” *arXiv preprint arXiv:1511.07289*, vol. 4, no. 5, p. 11, 2015.
- [38] N. Srivastava *et al.*, “Dropout: a simple way to prevent neural networks from overfitting,” *The journal of machine learning research*, 2014.
- [39] I. Loshchilov and F. Hutter, “Decoupled weight decay regularization,” *arXiv preprint arXiv:1711.05101*, 2017.
- [40] A. Agrawal *et al.*, “Differentiable convex optimization layers,” *Advances in neural information processing systems*, vol. 32, 2019.
- [41] P. J. Goulart and Y. Chen, “Clarabel: An interior-point solver for conic programs with quadratic objectives,” 2024.
- [42] W. Shao and V. Vittal, “Corrective switching algorithm for relieving overloads and voltage violations,” *IEEE Transactions on Power Systems*, vol. 20, no. 4, pp. 1877–1885, 2005.
- [43] Y. Hou *et al.*, “Research and application of dynamic line rating technology,” *Energy Reports*, vol. 6, pp. 716–730, 2020.